ARTICLE IN PRESS

Extreme Mechanics Letters ▮ (▮▮▮▮) ▮▮▮–▮▮▮

Contents lists available at ScienceDirect

Extreme Mechanics Letters

journal homepage: www.elsevier.com/locate/eml

Design of planar isotropic negative Poisson's ratio structures

Sicong Shan [a], Sung H. Kang [a,b], Zhenhao Zhao [a,c], Lichen Fang [a,c], Katia Bertoldi [a,d,*]

[a] School of Engineering and Applied Sciences, Harvard University, Cambridge, MA, 02138, USA

[b] Department of Mechanical Engineering and Hopkins Extreme Materials Institute, Johns Hopkins University, Baltimore, MD, 21218, USA

[c] School of Aerospace, Tsinghua University, Beijing, 100084, China

[d] Wyss Institute for Biologically Inspired Engineering, Harvard University, Cambridge, MA, 02138, USA

ARTICLE INFO

Article history:
Received 9 April 2015
Received in revised form 18 May 2015
Accepted 18 May 2015
Available online xxxx

Keywords:
Poisson's ratio
Auxetic
Isotropic

ABSTRACT

Most of the auxetic materials that have been characterized experimentally or studied analytically are anisotropic and this limits their possible applications, as they need to be carefully oriented during operation. Here, through a combined numerical and experimental approach, we demonstrate that 2D auxetic materials with isotropic response can be easily realized by perforating a sheet with elongated cuts arranged to form a periodic pattern with either six-fold or three-fold symmetry. Moreover, we also show that the auxetic behavior can be easily tuned by varying the length of the cuts and that it is retained even under large levels of applied deformation beyond the limit of small strains. This novel, simple and scalable design can serve as an important guideline for designing and fabricating isotropic auxetic materials that can have a significant impact on a wide range of applications.

1. Introduction

The Poisson's ratio (ν) is the ratio of transverse contraction strain to longitudinal extension strain in the direction of stretching force. Most materials are characterized by a positive Poisson's ratio ($\nu > 0$) and contract in the directions orthogonal to the applied tensile load. However, in the recent years natural materials with negative Poisson's ratio (also called auxetic materials) have been discovered [1–4]. Moreover, rationally designed geometries and structural mechanisms have also been reported to achieve negative Poisson's ratio. Examples include foams with re-entrant ribs [5–7], chiral microstructures [8,9], rotating units [10–14] and origami structures [15–17]. In all these demonstrations, careful design of the microstructure has led to effective negative macroscopic Poisson's ratios ($\nu < 0$), even though the bulk materials have a positive Poisson's ratio. Auxetic materials are attracting increasing interest because they are characterized by enhanced mechanical properties, such as increased shear modulus, indentation resistance and fracture toughness [5,18], and can achieve extremely large strains and shape changes [19].

Most of the auxetic materials that have been characterized experimentally or studied analytically are anisotropic [20] and exhibit different properties depending on the loading direction. While the anisotropy can result in larger negative values of Poisson's ratio [21,22], it also limits the application of auxetic materials, as they need to be carefully oriented during operation. In fact, failure to orient the structure may cause the material to exhibit a completely different behavior from the designed one. Therefore, to enable practical use of auxetic materials in real applications, it is crucial to design and develop isotropic auxetic materials and structures.

* Corresponding author at: School of Engineering and Applied Sciences, Harvard University, Cambridge, MA, 02138, USA.
E-mail address: bertoldi@seas.harvard.edu (K. Bertoldi).

http://dx.doi.org/10.1016/j.eml.2015.05.002
2352-4316/

Please cite this article in press as: S. Shan, et al., Design of planar isotropic negative Poisson's ratio structures, Extreme Mechanics Letters (2015), http://dx.doi.org/10.1016/j.eml.2015.05.002

Currently, there are few auxetic materials showing isotropic behavior. These include disordered systems such as foams [5], randomly oriented composite laminates [23], granular materials [24] and composites with randomly distributed inclusions [25,26]. Alternatively, to achieve better control and tunability of the Poisson's ratio, ordered auxetic isotropic systems have been numerically designed, such as hexagonal chiral honeycombs [8,9], intricate networks of rods, hinges and springs [27], two-phase composite materials with hexagonal symmetry [28], assemblies of flexible frames and rigid cores [29] and systems of hard cyclic hexamers [30]. Moreover, topology optimization has been used to identify periodic composites with auxetic and isotropic response [31]. Still, it remains a fundamental challenge to design isotropic material systems with controllable auxetic behavior that can be easily manufactured.

In this study, we report a new, simple and scalable approach to design and fabricate planar auxetic materials with isotropic behavior. Our starting points are the following two observations: (i) sheets with periodic arrays of elongated elliptical voids [12] and cuts [11,19,32,33] can exhibit auxetic behavior; (ii) two-dimensional crystalline lattices with six-fold or three-fold rotational symmetry are transversely isotropic [34,35]—i.e. isotropic in their transverse plane. Inspired by these facts, here we investigate the mechanical response of elastic sheets with embedded periodic arrays of elongated cuts and focus on the effect of the degree of rotational symmetry of the pattern. Remarkably, our numerical and experimental results demonstrate that 2D auxetic materials with isotropic response can be easily realized by perforating a sheet with elongated cuts arranged to form a periodic pattern with either six-fold or three-fold symmetry. Moreover, we also show that the auxetic behavior can be easily tuned by varying the length of the cuts and it is retained even under large levels of applied deformation beyond the limit of small strains.

2. Numerical simulations

To demonstrate our approach, we start by studying the mechanical response under uniaxial tension of elastomeric thin sheets with a kagome (see Fig. 1(b)) and square (see Fig. 1(c)) array of elongated cuts. The square array of cuts has been already shown to result in auxetic response [12], but since the pattern has four-fold symmetry we expect the response of the system to be anisotropic. By contrast, the kagome pattern has six-fold symmetry, so we conjecture its response to be both isotropic and auxetic. To test our hypothesis we characterize the mechanical response of the systems for different orientations of the cut pattern with respect to the loading direction, as shown in Fig. 1(b) and (c) for θ ranging between 0° and 45°.

We start by performing numerical simulations using the non-linear Finite Element (FE) code ABAQUS/Standard. In all our analysis the mechanical response of the elastomeric sheet is captured using a nearly incompressible Neo-Hookean material model with initial shear modulus μ_0 and an extremely high bulk modulus K_0 ($K_0/\mu_0 \approx 1000$). Since all considered structures are thin and planar, two dimensional finite-element models are constructed using six-node, quadratic, plane stress elements (ABAQUS element type CPS6M). The cuts are modeled as extremely elongated rhombi (with diagonals whose ratio is chosen to be 0.02) and the accuracy of the FE model is ensured by locally refining the mesh around the sharp angles of the cuts (where we use elements with edges of length $\approx L_0/160$). To reduce the computational cost and ensure the response is not affected by boundary effects, we consider two-dimensional, infinite periodic structures using representative volume elements (RVEs—see Fig. 2(a) and (b)) with suitable periodic boundary conditions [36,37]. Each model is loaded uniaxially by applying a finite macroscopic tensile strain in vertical direction, $\overline{\varepsilon}_{yy}$. The macroscopic Poisson's ratio with respect to the undeformed configuration, $\overline{\nu}$, is then obtained as $\overline{\nu} = -\overline{\varepsilon}_{xx}/\overline{\varepsilon}_{yy}$, where $\overline{\varepsilon}_{xx}$ is the resulting finite macroscopic strain in horizontal direction. Note that alternatively for largely deformed structures and materials the incremental Poisson's ratio (defined as the ratio of the partial derivatives of the two strains) can be used to characterize their lateral expansion/contraction [21,38]. The degree of anisotropy of each model is then examined by rotating the RVE by an angle θ, reapplying the tensile strain $\overline{\varepsilon}_{yy}$ in vertical direction and recalculating $\overline{\nu}$. In all our analysis we vary θ through the range [0°–180°] at intervals of 3°. Finally, we note that the length of the cuts, l, can vary between 0 and L_0, where L_0 is the length at which adjacent cuts start touching. In our simulations we vary l/L_0 between 0.1 and 0.9.

The numerical results for the square and kagome patterns are shown in Fig. 2. For each pattern we report the evolution of the Poisson's ratio, $\overline{\nu}$, as a function of the orientation angle, θ, for different values of cut length, l/L_0. First, we note that for both patterns $\overline{\nu}$ monotonously decreases from 0.5 to -1 as l/L_0 progressively increases. In particular, we find that $\overline{\nu} \sim 0$ for $l/L_0 \sim 0.5$. Therefore, our results indicate that $\overline{\nu}$ can be easily controlled by varying the cut-length. Remarkably, the numerical analysis also reveals that the response of the kagome pattern is isotropic, since $\overline{\nu}$ is not affected by the orientation of the pattern with respect to the loading. In stark contrast, the mechanical response of the square pattern depends on θ and $\overline{\nu}$ is found to be maximum for $\theta = 45°$ and 135° and minimum for $\theta = 0°$ and 90°. We also find that for the square pattern the extent of anisotropy is affected by l/L_0 and is particularly accentuated for $0.4 < l/L_0 < 0.7$. Note that this is the range of cut-lengths in which we are particularly interested, since for these intermediate values of l/L_0 the cuts can be effectively used to control $\overline{\nu}$. In fact, for $l/L_0 < 0.4$ the cuts do not affect significantly the response of the structure, so that its behavior is similar to that of the homogeneous elastic sheet with $\overline{\nu} \sim 0.5$. On the other hand, when $l/L_0 > 0.7$ the structure approximates a network of rigid polygons connected by rotating hinges, whose Poisson's ratio is known to be -1.0 [39]. Our results indicate that as l/L_0 approaches 1, even the square tiling behaves in an isotropic way. This is expected since networks of rigid polygons have a single degree of freedom and, therefore, their response is not affected by the direction of loading. However, for such large values of l/L_0 the integrity and strength of the structures is severely reduced, limiting their possible applications. Finally, we note from the results that $\overline{\nu}$ is not affected by the amount of applied deformation and that the structures remain auxetic even when largely deformed (i.e. $\overline{\varepsilon}_{yy} = 0.1$).

Please cite this article in press as: S. Shan, et al., Design of planar isotropic negative Poisson's ratio structures, Extreme Mechanics Letters (2015), http://dx.doi.org/10.1016/j.eml.2015.05.002

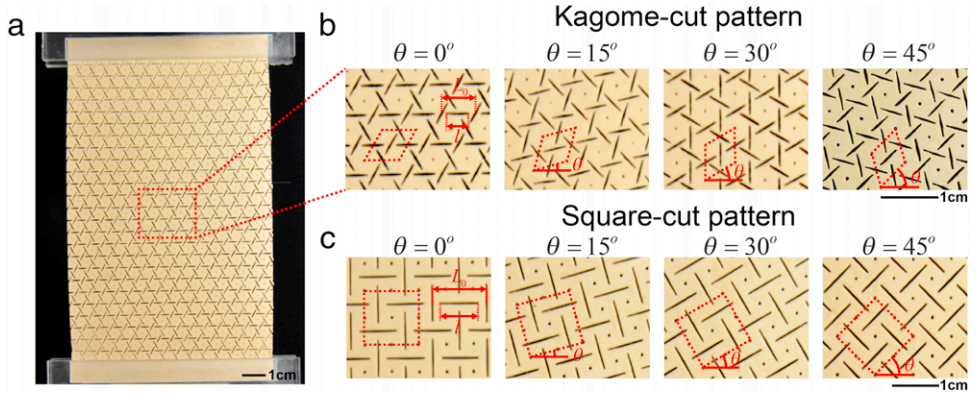

Fig. 1. 2D auxetic materials are realized by embedding a pattern of elongated cuts into an elastomeric sheet. (a) Snapshot of a sample with a kagome cut-pattern. To test whether the mechanical response of the system is isotropic, samples with the cut-pattern oriented at different angles θ with respect to the horizontal direction are tested uniaxially. (b) Zoom-in views of the central region of samples with a kagome cut-pattern for $\theta = 0^\circ, 15^\circ, 30^\circ, 45^\circ$. (c) Zoom-in views of the central region of samples with a square cut-pattern for $\theta = 0^\circ, 15^\circ, 30^\circ, 45^\circ$. Note that l is the length of cuts, while L_0 denotes the upper bound of l. The representative volume elements (RVEs) for both cut-patterns are outlined by red dashed lines. (For interpretation of the references to color in this figure legend, the reader is referred to the web version of this article.)

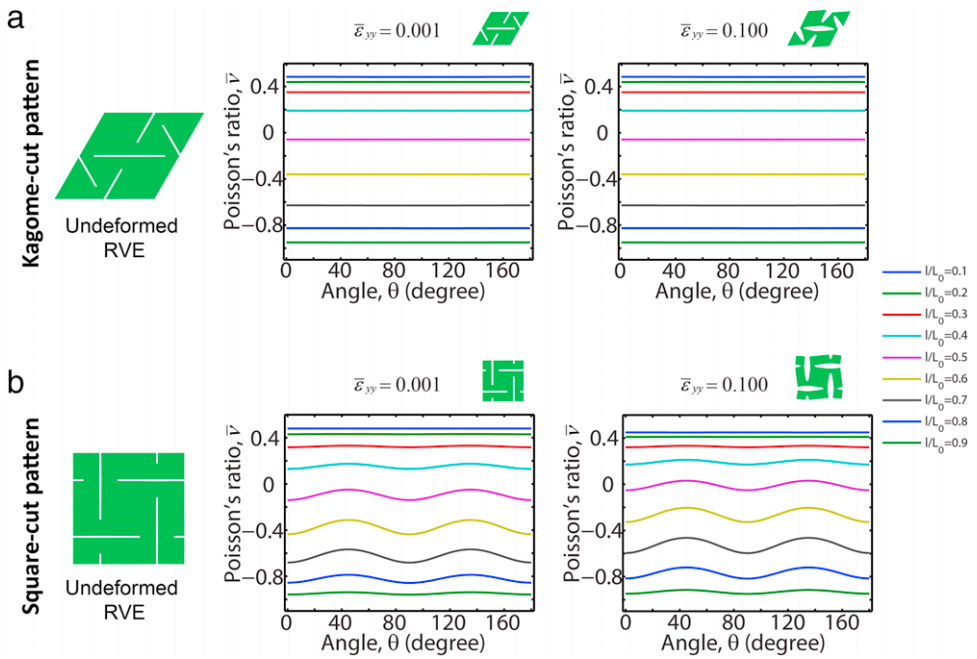

Fig. 2. Numerical predictions for the in-plane Poisson's ratio, $\bar{\nu}$, as a function of the orientation of the cut-pattern with respect to the loading direction. (a) Results for the kagome cut-pattern. (b) Results for the square cut-pattern. Results for both small ($\bar{\varepsilon}_{yy} = 0.001$) and large ($\bar{\varepsilon}_{yy} = 0.1$) values of applied strain are reported.

3. Experiments

To verify our numerical analysis, we build physical models of the kagome and square patterns. We start with sheets of natural latex rubber of size 87 mm × 145 mm and thickness 0.32 mm and use a high speed engraving laser system (*Kern Lasers Systems*) to fabricate the periodic array of cuts. In all our samples the cuts have an approximate width of ∼300 μm and L_0 (and therefore, the size of the RVE) is chosen so that each specimen comprises more than 10 RVEs to reduce the boundary effects. The cut-length is then determined to achieve $l/L_0 = 0.3,\ 0.5$ and 0.7. To quantify the degree of anisotropy of the structures, a series of samples are fabricated with patterns orientated at different angles with respect to the vertical direction (see Figs. 1 and 3). In particular, by taking advantage of the symmetry of the cut patterns, we fabricate samples characterized by $\theta = 0^\circ, 7.5^\circ, 15^\circ, 22.5^\circ, 30^\circ, 37.5^\circ, 45^\circ$ and 52.5° for the kagome lattice, while we consider $\theta = 0^\circ, 15^\circ, 30^\circ$ and 45° for the square lattice.

Uniaxial tensile tests are performed at room temperature on a standard quasi-static loading frame (In-

Please cite this article in press as: S. Shan, et al., Design of planar isotropic negative Poisson's ratio structures, Extreme Mechanics Letters (2015), http://dx.doi.org/10.1016/j.eml.2015.05.002

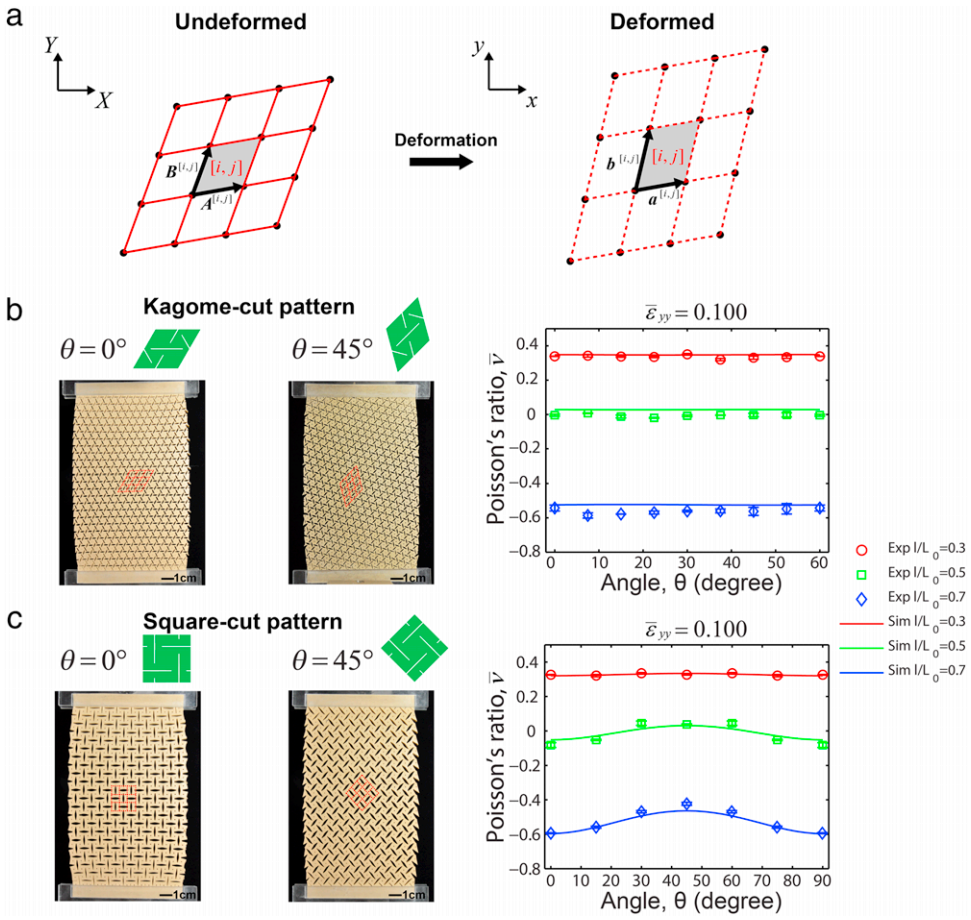

Fig. 3. Comparison between experimental and numerical results. (a) Schematic diagram of the central region with 9 RVEs, which are used to calculate $\overline{\nu}$. $\mathbf{A}^{[i,j]}$ and $\mathbf{B}^{[i,j]}$ are the lattice vectors spanning the RVE in undeformed state, while $\mathbf{a}^{[i,j]}$, $\mathbf{b}^{[i,j]}$ are the lattice vectors in the deformed state. (b) Comparison between experimental (markers) and numerical results (continuous lines) for the kagome cut-pattern. Experimental Poisson's ratio at $\theta = 0^\circ$ is also used for $\theta = 60^\circ$ for visualization purpose. (c) Comparison between experimental (markers) and numerical results (continuous lines) for the square cut-pattern. Snapshots of the samples with $\theta = 0^\circ$ and 45° at a tensile strain of $\overline{\varepsilon}_{yy} = 0.1$ are shown on the left. Experimental Poisson's ratio at $\theta = 0^\circ$, 15°, 30° is also used for $\theta = 90^\circ$, 75°, 60° for visualization purpose.

stron 5566) with a 1 kN load cell (Instron 2525-806) in a displacement-controlled manner. The samples are stretched using two custom-made fixtures to enhance gripping. In all the tests a displacement of 15.0 mm in vertical direction is applied (corresponding to a strain $\overline{\varepsilon}_{yy} = 0.1$) at a cross-head velocity of 0.15 mm/min, ensuring quasi-static loading conditions. To monitor the evolution of the deformation, small dots (with diameter <0.5 mm) are engraved to mark the vertices of the RVEs during the cutting step, as shown in Fig. 1. The position of the markers is recorded using a high-resolution digital camera (Nikon D90 SLR) and then analyzed by digital image processing (MATLAB). In particular, we focus on the behavior of nine RVEs in the central part of the samples, where the response is more uniform and not affected by boundary effects. For each RVE, macroscopic values of the finite strain, $\varepsilon_{xx}^{[i,j]}$ and $\varepsilon_{yy}^{[i,j]}$, are calculated from the positions of the markers. In fact, if we denote with $\mathbf{A}^{[i,j]}$, $\mathbf{B}^{[i,j]}$ and $\mathbf{a}^{[i,j]}$, $\mathbf{b}^{[i,j]}$ the two lattice vectors spanning the RVE in the undeformed and deformed configurations, respectively, it follows that (see *Supporting Information* for details)

$$\begin{pmatrix} \varepsilon_{xx}^{[i,j]} + 1 & \varepsilon_{xy}^{[i,j]} \\ \varepsilon_{yx}^{[i,j]} & \varepsilon_{yy}^{[i,j]+1} \end{pmatrix} = \begin{pmatrix} a_x^{[i,j]} & b_x^{[i,j]} \\ a_x^{[i,j]} & b_y^{[i,j]} \end{pmatrix} \begin{pmatrix} A_x^{[i,j]} & B_y^{[i,j]} \\ A_x^{[i,j]} & B_y^{[i,j]} \end{pmatrix}^{-1} \tag{1}$$

where the components of the lattice vectors in x- and y-directions can be easily calculated from the positions of the markers. For each RVE macroscopic values of the Poisson's ratio with respect to the undeformed configuration are then obtained as

$$\nu^{[i,j]} = -\frac{\epsilon_{xx}^{[i,j]}}{\epsilon_{yy}^{[i,j]}}, \tag{2}$$

and finally the ensemble average, $\overline{\nu} = \langle \nu^{[i,j]} \rangle$, of the nine central RVEs under consideration is computed.

In Fig. 3 we report the experimentally measured Poisson's ratio, $\overline{\nu}$, as a function of the orientation of the pattern for the kagome and square array of cuts. The experimental

Please cite this article in press as: S. Shan, et al., Design of planar isotropic negative Poisson's ratio structures, Extreme Mechanics Letters (2015), http://dx.doi.org/10.1016/j.eml.2015.05.002

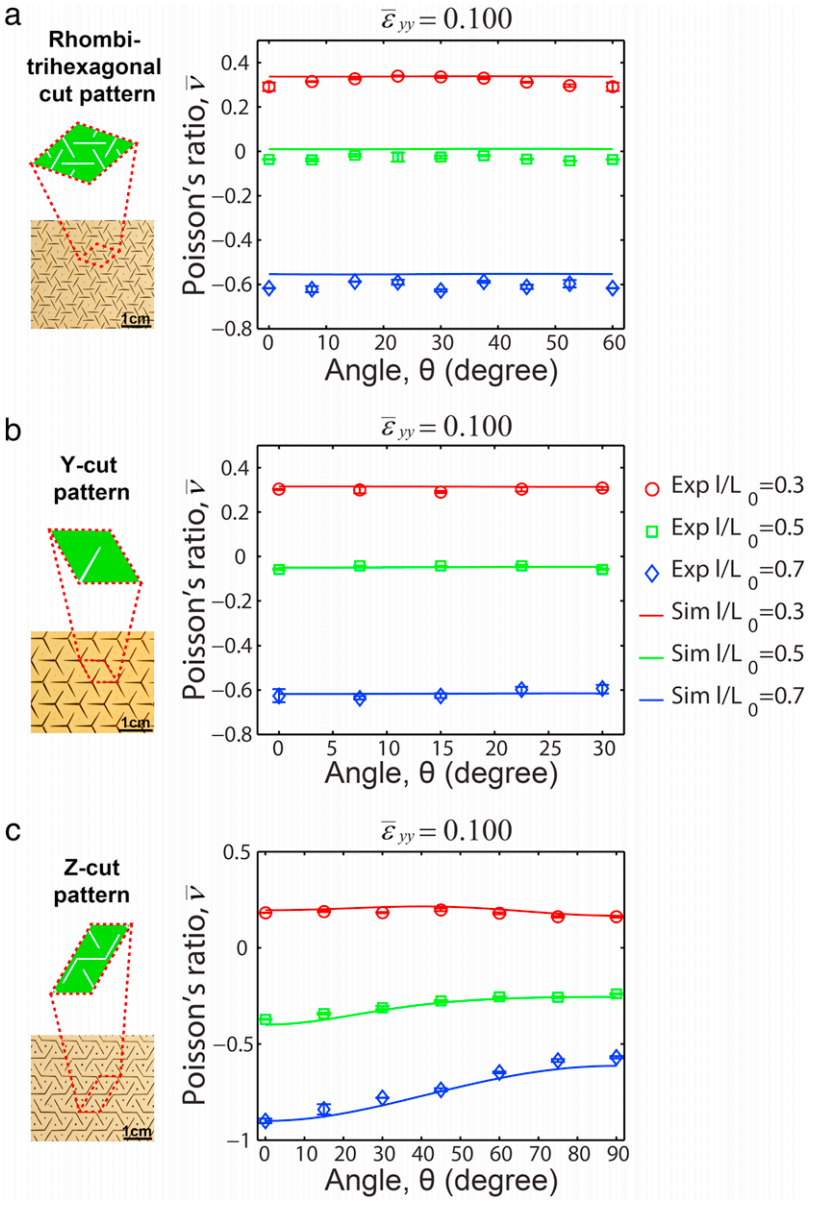

Fig. 4. Comparison between experimental and numerical results. (a) Comparison between experimental (markers) and numerical results (continuous lines) for the rhombitrihexagonal cut-pattern. (b) Comparison between experimental (markers) and numerical results (continuous lines) for the Y cut-pattern. (c) Comparison between experimental (markers) and numerical results (continuous lines) for the Z cut-pattern.

results (markers) are compared to the numerical predictions (continuous lines), showing excellent agreement and confirming the validity of our numerical analysis. Again, we note that the kagome cut-pattern exhibits nearly identical Poisson's ratio in all loading directions, regardless of the cut-length. By contrast, the square cut-pattern exhibits an orientation-dependent Poisson's ratio, except for short cuts ($l/L_0 = 0.3$) when the response of the material is similar to that of the homogeneous elastic sheet.

4. Discussion and conclusions

Having demonstrated our method for kagome and square patterns (with 6-fold and 4-fold rotational symmetry, respectively), we now show that the approach can be generalized to arbitrary cut-patterns. In particular, in Fig. 4 we report experimental and numerical results for a rhombitrihexagonal cut-pattern, a Y cut-pattern and a Z cut-pattern. Again, we observe the excellent agreement between all numerical (markers) and experimental (continuous lines) results. As expected, since the rhombitrihexagonal cut-pattern and Y cut-pattern have six-fold and three-fold rotational symmetry, for these structures the response is found to be isotropic for all values of l/L_0 and even at large strain levels. Differently, the Z cut-pattern exhibits strong anisotropy and its Poisson's ratio for $l/L_0 = 0.7$ varies from -0.57 to -0.90 when the loading direction changes. This behavior is expected since the Z-pattern

Please cite this article in press as: S. Shan, et al., Design of planar isotropic negative Poisson's ratio structures, Extreme Mechanics Letters (2015), http://dx.doi.org/10.1016/j.eml.2015.05.002

has two-fold rotational symmetry. Finally, all our results demonstrate that the cut-length can be effectively used to tune the Poisson's ratio of the system. Simply by increasing l/L_0 from 0.3 to 0.7, $\overline{\nu}$ is significantly reduced from $\sim$0.3 to ~ -0.6, giving us the opportunity to easily realize auxetic systems. Therefore, our results confirm the robustness of our approach. By patterning elastic sheets with arrays of cuts, we can achieve not only negative Poisson's ratio, but also isotropic behavior by carefully choosing the degree of rotational symmetry of the pattern.

In summary, our findings demonstrate a fundamentally new way of generating isotropic 2D materials with negative Poisson's ratio by embedding periodic arrays of cuts in elastomeric sheets. Interestingly, we showed that the Poisson's ratio of the system can be easily tuned and drastically altered by varying the length of the cuts, while the isotropy of the system is controlled by the degree of rotational symmetry of the cut-patterns. Combining numerical analysis and experiments, we investigated the response of five different cut-patterns and found that patterns with three- and six-fold symmetry result in an isotropic response, while arrays of cuts with two- and four-fold symmetry lead to anisotropic responses. Remarkably, the systems we have explored can be easily fabricated and have a robust behavior. We believe that the insights gained in this study can serve as an important guideline for designing and fabricating isotropic auxetic materials that can have a significant impact on a wide range of applications.

Acknowledgments

This work has been supported by NSF Harvard MRSEC through grant DMR-1420570 and grant CMMI-1149456 (CAREER) and by the Wyss Institute through the Seed Grant Program. K.B. acknowledges start-up funds from the Harvard School of Engineering and Applied Sciences and the support of the Kavli Institute at Harvard University.

Competing Interests. The authors declare that they have no competing financial interests.

Appendix A. Supplementary data

Supplementary material related to this article can be found online at http://dx.doi.org/10.1016/j.eml.2015.05.002.

References

[1] R. Baughman, J. Shacklette, A. Zakhidov, S. Stafstrom, Negative Poisson's ratios as a common feature of cubic metals, Nature 392 (1998) 362–365.
[2] J.N. Grima, R. Jackson, A. Alderson, K. Evans, Do zeolites have negative Poisson's ratios? Adv. Mater. 12 (24) (2000) 1912–1918.
[3] F. Song, J. Zhou, X. Xu, Y. Xu, Y. Bai, Effect of a negative Poisson ratio in the tension of ceramics, Phys. Rev. Lett. 100 (2008) 245502.
[4] N.R. Keskar, J.R. Chelikowsky, Negative Poisson ratios in crystalline SiO_2 from first-principles calculations, Nature 358 (1992) 222–224.
[5] R.S. Lakes, Foam structures with a negative Poisson's ratio, Science 235 (4792) (1987) 1038–1040.
[6] J. Choi, R. Lakes, Non-linear properties of polymer cellular materials with a negative Poisson's ratio, J. Mater. Sci. 27 (17) (1992) 4678–4684.
[7] J. Schwerdtfeger, F. Schury, M. Stingl, F. Wein, R. Singer, C. Körner, Mechanical characterisation of a periodic auxetic structure produced by SEBM, Phys. Status Solidi b 249 (2012) 1347–1352.
[8] F. Scarpa, S. Blain, T. Lew, D. Perrott, M. Ruzzene, J. Yates, Elastic buckling of hexagonal chiral cell honeycombs, Compos. Part A - Appl. Sci. 38 (2) (2007) 280–289.
[9] D. Prall, R. Lakes, Properties of a chiral honeycomb with a Poisson's ratio of -1, Int. J. Mech. Sci. (ISSN: 0020-7403) 39 (3) (1997) 305–314.
[10] E. Chetcuti, B. Ellul, E. Manicaro, J. Brincat, D. Attard, R. Gatt, J. Grima, Modeling auxetic foams through semi-rigid rotating triangles, Phys. Status Solidi (b) 251 (2) (2014) 297–306.
[11] R. Gatt, L. Mizzi, J. Azzopardi, K. Azzopardi, D. Attard, A. Casha, J. Briffa, J. Grima, Hierarchical auxetic mechanical metamaterials, Sci. Rep. 5 (2015) 8395.
[12] M. Taylor, L. Francesconi, M. Gerendás, A. Shanian, C. Carson, K. Bertoldi, Low porosity metallic periodic structures with negative Poisson's ratio, Adv. Mater. 26 (15) (2014) 2365–2370.
[13] K. Bertoldi, P. Reis, S. Willshaw, T. Mullin, Negative Poisson's ratio behavior induced by an elastic instability, Adv. Mater. 22 (2010) 361–366.
[14] H. Mitschke, J. Schwerdtfeger, F. Schury, M. Stingl, C. Körner, R. Singer, V. Robins, K. Mecke, G. Schröder-Turk, Finding auxetic frameworks in periodic tessellations, Adv. Mater. 23 (22–23) (2011) 2669–2674.
[15] K. Miura, Method of packaging and deployment of large membranes in space, in: The Institute of Space and Astronautical Science-Japan Aerospace Exploration Agency, 1985, pp. 1–9.
[16] Z. Wei, Z. Guo, L. Dudte, H. Liang, L. Mahadevan, Geometric mechanics of periodic pleated origami, Phys. Rev. Lett. 110 (2013) 215501.
[17] M. Schenk, S. Guest, Geometry of Miura-folded metamaterials, Proc. Natl. Acad. Sci. USA 110 (2013) 3276–3281.
[18] K.E. Evans, M.A. Nkansah, I.J. Hutchinson, S.C. Rogers, Molecular network design, Nature 353 (1991) 124.
[19] Y. Cho, J. Shin, A. Costa, T. Kim, V. Kunin, J. Li, S. Lee, S. Yang, H. Han, I. Choi, D. Srolovitz, Engineering the shape and structure of materials by fractal cut, Proc. Natl. Acad. Sci. USA 111 (49) (2014) 17390–17395.
[20] J. Lee, J. Singer, E. Thomas, Micro-/nanostructured mechanical metamaterials, Adv. Mater. 24 (36) (2012) 4782–4810.
[21] B. Caddock, K. Evans, Microporous materials with negative Poisson's ratios. I. Microstructure and mechanical properties, J. Phys. D: Appl. Phys. 22 (12) (1989) 1877.
[22] T. Ting, T. Chen, Poisson's ratio for anisotropic elastic materials can have no bounds, Quart. J. Mech. Appl. Math. 58 (1) (2005) 73–82.
[23] H. Yeh, R. Zhang, A study of negative Poisson's ratio in randomly oriented quasi-isotropic composite laminates, J. Compos. Mater. 33 (19) (1999) 1843–1857.
[24] J. Richard, R. Leo, Note on a random isotropic granular material with negative Poisson's ratio, Internat. J. Engrg. Sci. 26 (4) (1988) 373–383.
[25] H. Xiaonan, H. Hong, S. Vadim, A novel concept to develop composite structures with isotropic negative Poisson's ratio: Effects of random inclusions, Compos. Sci. Technol. 72 (15) (2012) 1848–1854.
[26] X. Hou, H. Hu, V. Silberschmidt, Numerical analysis of composite structure with in-plane isotropic negative Poisson's ratio: Effects of materials properties and geometry features of inclusions, Compos. Part—Eng. 58 (2014) 152–159.
[27] R. Almgren, An isotropic three-dimensional structure with Poisson's ratio = -1, J. Elasticity 15 (4) (1985) 427–430.
[28] G.W. Milton, Composite materials with Poisson's ratios close to -1, J. Mech. Phys. Solids 40 (5) (1992) 1105–1137.
[29] I. Shufrin, E. Pasternak, A. Dyskin, Planar isotropic structures with negative Poisson's ratio, Int. J. Solids Struct. 49 (17) (2012) 2239–2253.
[30] K. Wojciechowski, A. Branka, Negative Poisson ratio in a two-dimensional isotropic" solid, Phys. Rev. A 40 (1989) 7222–7225.
[31] U. Larsen, O. Sigmund, S. Bouwstra, Design and fabrication of compliant micromechanisms and structures with negative Poisson's ratio, in: IEEE, The Ninth Annual International Workshop on Micro Electro Mechanical Systems, 1996, MEMS'96, Proceedings. An Investigation of Micro Structures, Sensors, Actuators, Machines and Systems, 1996, pp. 365–371.
[32] O. Sigmund, Materials with prescribed constitutive parameters: An inverse homogenization problem, Int. J. Solids Struct. (ISSN: 0020-7683) 31 (17) (1994) 2313–2329.
[33] A. Slann, W. White, F. Scarpa, K. Boba, I. Farrow, Cellular plates with auxetic rectangular perforations, Phys. Status Solidi B (2015).

Please cite this article in press as: S. Shan, et al., Design of planar isotropic negative Poisson's ratio structures, Extreme Mechanics Letters (2015), http://dx.doi.org/10.1016/j.eml.2015.05.002

[34] L. Landau, E. Lifshitz, A. Kosevich, L. Pitaevski, Theory of Elasticity, in: Course of Theoretical Physics, Butterworth-Heinemann, 1986.
[35] R. Newnham, Properties of Materials: Anisotropy, Symmetry, Structure: Anisotropy, Symmetry, Structure, OUP, Oxford, 2004.
[36] K. Bertoldi, M.C. Boyce, S. Deschanel, S.M. Prange, T. Mullin, Mechanics of deformation-triggered pattern transformations and superelastic behavior in periodic elastomeric structures, J. Mech. Phys. Solids 56 (8) (2008) 2642–2668.
[37] M. Danielsson, D. Parks, M. Boyce, Three-dimensional micromechanical modeling of voided polymeric materials, J. Mech. Phys. Solids 50 (2) (2002) 351–379.
[38] J. Shim, S. Shan, A. Kosmrlj, S. Kang, E. Chen, J. Weaver, K. Bertoldi, Harnessing instabilities for design of soft reconfigurable auxetic/chiral materials, Soft Matter 9 (2013) 8198–8202.
[39] J. Grima, A. Alderson, K. Evans, Auxetic behaviour from rotating rigid units, Phys. Status Solidi b 242 (3) (2005) 561–575.

Please cite this article in press as: S. Shan, et al., Design of planar isotropic negative Poisson's ratio structures, Extreme Mechanics Letters (2015), http://dx.doi.org/10.1016/j.eml.2015.05.002

Supporting Information for
Design of Planar Isotropic Structures with Negative Poisson's Ratio

Sicong Shan,[1] Sung H. Kang,[1,2] Zhenhao Zhao,[1,3] Lichen Fang,[1,3] and Katia Bertoldi[1,4]

[1]*School of Engineering and Applied Sciences, Harvard University, Cambridge, MA 02138, USA.*
[2]*Department of Mechanical Engineering and Hopkins Extreme Materials Institute, Johns Hopkins University, Baltimore, Maryland, 21218, USA.*
[3]*School of Aerospace, Tsinghua University, Beijing, 100084, China.*
[4]*Kavli Institute for Bionano Science and Technology, Harvard University, Cambridge, MA 02138, USA.*

FABRICATION

We first describe the response of the material we used to fabricate our samples, then provide a summary of all samples we fabricated for this study.

Material

Natural latex rubber was used to fabricate the experimental samples for this study. The material was purchased in sheet form (1/8 inch thick) from McMaster Carr. The response of the elastic sheets was tested under uniaxial tension. The experimentally measured stress-strain curve is reported in Fig. S1 (red line), from which the initial shear modulus was measured to be $\mu_0 = 0.38$ MPa.

The observed constitutive behavior is modeled as hyperelastic. Let $\mathbf{F} = \frac{\partial \mathbf{x}}{\partial \mathbf{X}}$ be the deformation gradient, mapping a material point from the reference position $\mathbf{X}$ to its current location $\mathbf{x}$ and J be its determinant, $J = \det\mathbf{F}$. For an isotropic hyperelastic material the strain energy density W can be expressed as a function of the invariants of the right Cauchy-Green tensor $\mathbf{C} = \mathbf{F}^T\mathbf{F}$ (or, alternatively, also the left Cauchy-Green tensor $\mathbf{B} = \mathbf{F}\mathbf{F}^T$). In particular, the behavior of nearly incompressible materials is effectively described by splitting the deformation locally into volume-changing ($J^{1/3}\mathbf{I}$) and distortional ($\overline{\mathbf{F}}$) components as

$$\mathbf{F} = (J^{1/3}\mathbf{I})\overline{\mathbf{F}}, \tag{S1}$$

where $\mathbf{I}$ denotes the identity matrix.

The response of the latex rubber's is modeled using a Neo-Hookean hyperelastic material model, modified to include compressibility (with a high bulk modulus).

$$W = \frac{\mu_0}{2}(\overline{I}_1 - 3) + \frac{K_0}{2}(J-1)^2, \tag{S2}$$

where μ_0 and K_0 are the initial shear and bulk moduli and $\overline{I}_1 = \mathrm{tr}(\overline{\mathbf{F}}^T\overline{\mathbf{F}})$. The nominal (first Piola-Kirchoff) stress is then given by

$$\mathbf{S} = \frac{\partial W}{\partial \mathbf{F}} = \left[\mu_0 \mathrm{dev}\overline{\mathbf{B}} + K_0 J(J-1)\right]\mathbf{F}^{-T}, \tag{S3}$$

where $\overline{\mathbf{B}} = \overline{\mathbf{F}}\overline{\mathbf{F}}^T$ and dev is the deviatoric operator.

In all our simulations we used $K_0/\mu_0 \approx 2500$. Fig. S1 shows that the Neo-Hookean model captures the behavior well up to a nominal strain of about 0.8 which covers the majority of the strain levels studied.

Summary of fabricated samples

In Table I we provide a list of all samples fabricated and tested for this study.

Note that we took advantage of the symmetry of the cut patterns to reduce the number of samples to be fabricated, as shown in Fig. S2. In fact, for a cut pattern with N-fold rotational symmetry only values of θ within the interval $[0,\ 2\pi/N]$ need to be considered. Furthermore, for patterns with mirror symmetry the range of orientations to be

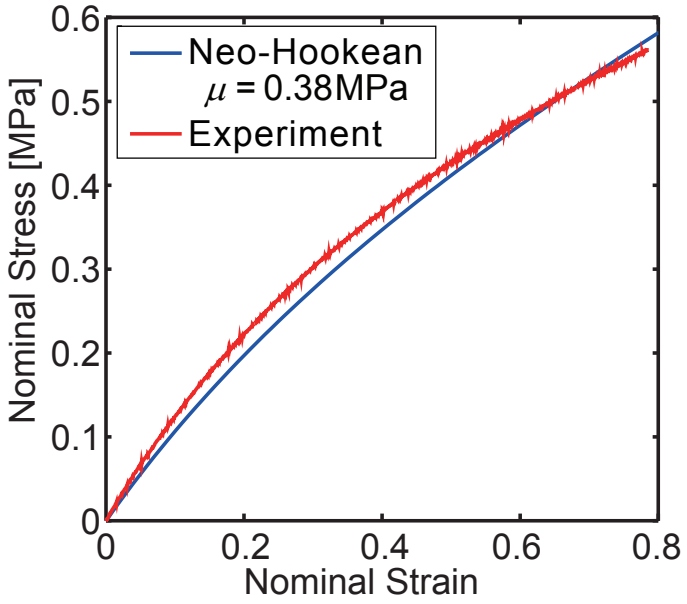

Figure S1: Nominal stress versus nominal strain in uniaxial tension for the rubber sheet. Comparison between experimental data and model predictions.

	$kagome-cut$	$square-cut$	$rhombi-trihexagonal-cut$	$Y-cut$	$Z-cut$
Rotational symmetry	6-fold	4-fold	6-fold	3-fold	2-fold
Axis of symmetry	0	2	0	3	2
θ_{min}	0°	0°	0°	0°	0°
θ_{max}	60°	45°	60°	30°	90°
$\Delta\theta$	7.5°	15°	7.5°	7.5°	15°

Table I: List of all samples fabricated and tested for this study. Note that the symmetry is determined on an infinitely large cut pattern and not on the RVE.

considered is further reduced to $[0, \pi/N]$. Operationally, for each pattern we varied θ through the range $[\theta_{min}, \theta_{max}]$ at interval $\Delta\theta$, where θ_{min}, θ_{max} and $\Delta\theta$ are specified in Table I. Note that for the Y-cut pattern we also took advantage of the rotational symmetry of the uniaxial loading conditions and used $\theta_{min} = 0°$ and $\theta_{max} = 30°$.

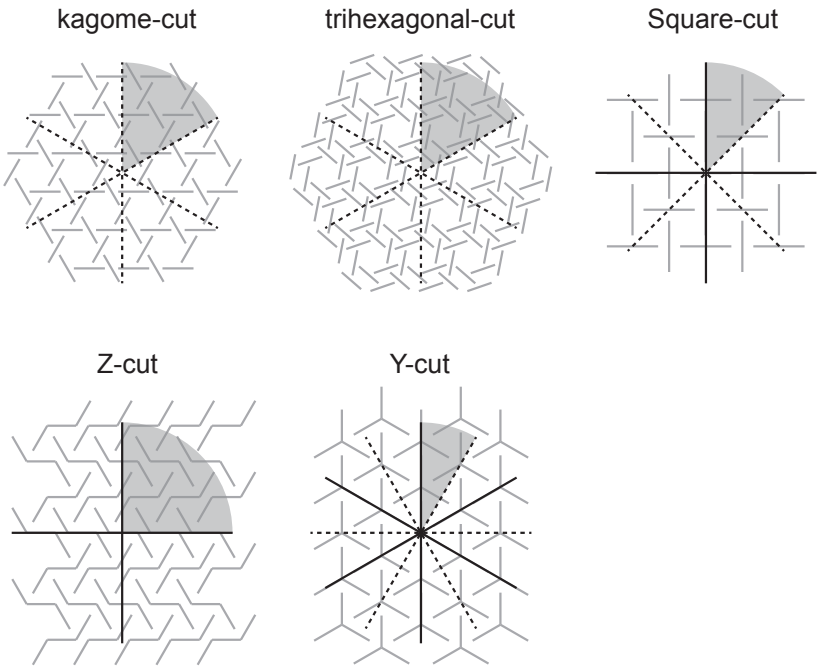

Figure S2: Cut patterns considered in our study. The grey are indicates the range of orientation angles used to investigate the response of each cut pattern. The solid lines are the axis of mirror symmetry, while the dashed lines indicate the rotational symmetry.

TESTING

In this section we describe in detail the procedure we used to calculate the Poisson's ratio, $\overline{\nu}$, from the experimental tests.

Calculation of Poisson's ratio from experiments

To quantify the deformation (and thus the Poisson's ratio, $\overline{\nu}$) taking place in the porous structures during the experiments, small marker dots (with diameter$< 0.5mm$) were engraved to mark the vertices of the RVEs during the cutting step, as shown in Fig. 1 in the main text. The position of the markers was recorded using a high resolution digital camera (Nikon D90 SLR) and then analyzed by digital image processing (Matlab). In particular, we focused on the behavior of 9 RVEs in the central part of the samples, where the response is more uniform and not affected by boundary effects. The markers at the corners of the chosen RVEs were identified in the initial frame, and followed through the loading process.

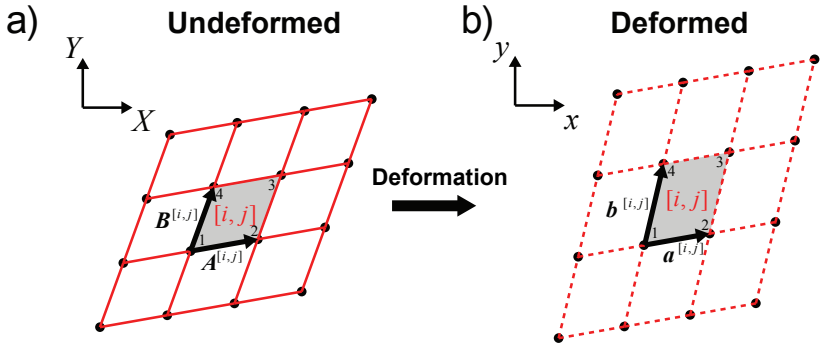

Figure S3: Schematic diagram of the central region with 9 RVEs, which are used to calculate $\overline{\nu}$. $\mathbf{A}^{[i,j]}$ and $\mathbf{B}^{[i,j]}$ are the lattice vectors spanning the RVE in undeformed state, while $\mathbf{a}^{[i,j]}$, $\mathbf{b}^{[i,j]}$ are the lattice vectors in the deformed state.

For each RVE, local homogenized values of the engineering strain $\varepsilon_{xx}^{[i,j]}$ and $\varepsilon_{yy}^{[i,j]}$, using the fact that the lattices vectors spanning the RVE in the deformed and undeformed configuration are related through the deformation gradient, $\mathbf{F}^{[i,j]}$, as

$$\mathbf{a}^{[i,j]} = \mathbf{F}^{[i,j]}\mathbf{A}^{[i,j]}, \qquad \mathbf{b}^{[i,j]} = \mathbf{F}^{[i,j]}\mathbf{B}^{[i,j]} \tag{S4}$$

where

$$\mathbf{F}^{[i,j]} = \begin{pmatrix} \varepsilon_{xx}^{[i,j]} + 1 & \varepsilon_{xy}^{[i,j]} \\ \varepsilon_{yx}^{[i,j]} & \varepsilon_{yy}^{[i,j]} + 1 \end{pmatrix} \tag{S5}$$

Note that the the lattice vectors in Eq. (S4) can be easily calculated from the positions of the markers as

$$\mathbf{A}^{[i,j]} = \begin{pmatrix} A_x^{[i,j]} \\ A_y^{[i,j]} \end{pmatrix} = \frac{1}{2}\begin{pmatrix} X_2^{[i,j]} - X_1^{[i,j]} + X_3^{[i,j]} - X_4^{[i,j]} \\ Y_2^{[i,j]} - Y_1^{[i,j]} + Y_3^{[i,j]} - Y_4^{[i,j]} \end{pmatrix} \tag{S6}$$

$$\mathbf{B}^{[i,j]} = \begin{pmatrix} B_x^{[i,j]} \\ B_y^{[i,j]} \end{pmatrix} = \frac{1}{2}\begin{pmatrix} X_4^{[i,j]} - X_1^{[i,j]} + X_3^{[i,j]} - X_2^{[i,j]} \\ Y_4^{[i,j]} - Y_1^{[i,j]} + Y_3^{[i,j]} - Y_2^{[i,j]} \end{pmatrix} \tag{S7}$$

$$\mathbf{a}^{[i,j]} = \begin{pmatrix} a_x^{[i,j]} \\ a_y^{[i,j]} \end{pmatrix} = \frac{1}{2}\begin{pmatrix} x_2^{[i,j]} - x_1^{[i,j]} + x_3^{[i,j]} - x_4^{[i,j]} \\ y_2^{[i,j]} - y_1^{[i,j]} + y_3^{[i,j]} - y_4^{[i,j]} \end{pmatrix} \tag{S8}$$

$$\mathbf{b}^{[i,j]} = \begin{pmatrix} b_x^{[i,j]} \\ b_y^{[i,j]} \end{pmatrix} = \frac{1}{2} \begin{pmatrix} x_4^{[i,j]} - x_1^{[i,j]} + x_3^{[i,j]} - x_2^{[i,j]} \\ y_4^{[i,j]} - y_1^{[i,j]} + y_3^{[i,j]} - y_2^{[i,j]} \end{pmatrix} \tag{S9}$$

where $(X_\alpha^{[i,j]}, Y_\alpha^{[i,j]})$ and $(x_\alpha^{[i,j]}, y_\alpha^{[i,j]})$ denote the coordinated of the α-th vertex of the RVE in the undeformed and deformed configuration, respectively.

Finally, local homogenized values of the engineering strain for the RVE can be obtained as

$$\mathbf{F}^{[i,j]} = \begin{pmatrix} \varepsilon_{xx}^{[i,j]} + 1 & \varepsilon_{xy}^{[i,j]} \\ \varepsilon_{yx}^{[i,j]} & \varepsilon_{yy+1}^{[i,j]} \end{pmatrix} = \begin{pmatrix} a_x^{[i,j]}, & b_x^{[i,j]} \\ a_x^{[i,j]}, & b_y^{[i,j]} \end{pmatrix} \begin{pmatrix} A_x^{[i,j]}, & B_y^{[i,j]} \\ A_x^{[i,j]}, & B_y^{[i,j]} \end{pmatrix}^{-1} \tag{S10}$$

$$= \frac{1}{A_x^{[i,j]} B_y^{[i,j]} - B_x^{[i,j]} A_y^{[i,j]}} \begin{pmatrix} a_x^{[i,j]} B_y^{[i,j]} - b_x^{[i,j]} A_y^{[i,j]}, & -a_x^{[i,j]} B_x^{[i,j]} + b_x^{[i,j]} A_x^{[i,j]} \\ a_y^{[i,j]} B_y^{[i,j]} - b_y^{[i,j]} A_y^{[i,j]}, & -a_y^{[i,j]} B_x^{[i,j]} + b_y^{[i,j]} A_x^{[i,j]} \end{pmatrix} \tag{S11}$$

since

$$\begin{pmatrix} A_x^{[i,j]}, & B_y^{[i,j]} \\ A_x^{[i,j]}, & B_y^{[i,j]} \end{pmatrix}^{-1} = \frac{1}{A_x^{[i,j]} B_y^{[i,j]} - B_x^{[i,j]} A_y^{[i,j]}} \begin{pmatrix} B_y^{[i,j]}, & -B_x^{[i,j]} \\ -A_y^{[i,j]}, & A_x^{[i,j]} \end{pmatrix} \tag{S12}$$

The local values of the engineering strain are then used to calculate local values of the Poisson's ratio as

$$\nu^{[i,j]} = -\frac{\varepsilon_{xx}^{[i,j]}}{\varepsilon_{yy}^{[i,j]}}, \tag{S13}$$

and finally the ensemble average, $\overline{\nu} =< \nu^{[i,j]} >$ of the nine central RVEs under consideration is computed.